Magnetic Small-angle Neutron Scattering

1. Introduction

Small Angle Neutron Scattering (SANS) is a technique that allows characterizing structures or objects on the nanometer scale, typically in the range between 1 nm and 150 nm. The information one can extract from SANS is primarily the average size, size distribution and spatial correlation of nanoscale structures, as well as shape and internal structure of particles (e.g. core-shell structure). Further, the scattering intensity on an absolute scale contains the product of scattering contrast of the investigated structures in the surrounding medium, and number or volume density. If one of both quantities is known, the other one can be derived in addition to the information mentioned before. All in all, SANS is a valuable technique, widely used in many fields, to characterize particles (in solution or in bulk), clusters, (macro-)molecules, voids and precipitates in the nanometer size range. Further, in-situ measurements allow following the temporal development and dynamics of such structures, on a time scale ranging from microseconds (stroboscopic) to hours.

Besides the nuclear interaction, due to their magnetic moment neutrons undergo a magnetic interaction with matter, approximately equally strong (in terms of order of magnitude) as the nuclear interaction. This property distinguishes neutrons markedly from x-rays where magnetic interaction is very weak and difficult to access experimentally. With this dual interaction of neutrons with matter they offer the opportunity to study both, compositional and magnetic structures and correlations. Thus, a strong area of application of neutrons traditionally was and still is the area of magnetism in solid state physics and condensed matter research. SANS in particular, probing structures on the nanometer scale, finds applications in micromagnetism, to magnetic clusters embedded in a solid nonmagnetic matrix, magnetic clusters suspended in fluids (e.g. ferrofluids), magnetism in nanostructured materials, vortex lattices in superconductors and many others. Further, by using a polarized neutron beam, very specific information on the magnetic structure or alignment of nanoparticles can be obtained, as well as on their response to an external magnetic field. In general, neutrons are the only probe which give direct access to magnetic moments and magnetic interactions and alignment down to the atomic scale, and the probing does not by itself impose a magnetic perturbance, as e.g. by an external magnetic field.

1.1 Neutron beams

Neutron beams for materials science and condensed matter research are produced either by nuclear reactors, with the most prominent representative being the ILL, Grenoble (F), or by neutron spallation sources, like ISIS, Abington (UK), the latter operating in pulsed mode. The neutron energy spectra provided at these sources, generated by specially tailored moderation systems, are primarily in the range of thermal energies with a Maxwellian distribution around 320 K (thermal neutrons) or 30 to 40 K (cold neutrons). The corresponding wavelengths of the neutron beams peak around 0.13 nm (thermal) or 0.3 to 0.4 nm (cold), both with a considerable tail towards higher wavelengths, in the case of cold neutrons reaching far beyond 1 nm. Thus, the wavelength range of neutron beams overlaps well with that of x-ray beams, being the basis of the similarities and complementarities of both types of probing beams for structural analysis. The difference lies in the type of response or interaction with materials: the x-rays are scattered by the electron clouds, resulting in a linear dependence of the scattering strength (scattering amplitude) on the atomic number. In contrast, neutrons are scattered at the atomic nuclei, and the nuclear scattering lengths vary more or less unsystematically for the different elements, and also distinguish different isotopes of one element. Further, as outlined before, neutrons undergo magnetic interaction with matter, which makes them a valuable probe for magnetic structures.

1.2 Atomic scattering amplitudes

The scattering amplitudes for nuclear scattering are widely tabulated, for the elements in natural isotopic abundance as well as for the individual isotopes [1]. The atomic scattering amplitudes for magnetic scattering will depend upon the atomic magnetic moment which includes implicitly the magnetic form factor descriptive of the spatial origin of the atomic magnetic moment. Values for the most prominent magnetic elements, like Fe, Co, Ni, Gd, can be found in [2]. For more complex systems, like alloys containing magnetic elements, the individual atomic magnetic moments may depend on the local magnetic surrounding and would have to be determined experimentally for each case. Examples for the Fe-Cr-, Ni-Fe- and Co-Cr-series can be found in [3].

1.3 The classical SANS instrument

The classical concept of a SANS instrument at a continuous neutron source was first realised in the early 1970's at the Jülich Research Centre, Germany, the ILL Grenoble, France [4] and the HFIR reactor in Oak Ridge, USA [5]. Modern instruments of this type, like the D22 instrument at the ILL, the SANS at HMI, Berlin, Germany, or the SINQ-SANS at PSI, Switzerland [6], still follow the same principle concept, although using state-of-the-art components and advanced technical concepts. For measurements of magnetic structures polarisation and spin-flipping of the incident beam is a viable option at HMI [7], GKSS, Geesthacht (D) [8], NIST, Gaithersburg (USA) LLB, Saclay (F) [9] and PSI, Villigen (CH).

The basic layout of a classical SANS instrument is illustrated in Figure 1. The preferential position of the instrument is at the end of a neutron guide supplying a spectrum of cold neutrons. The neutron energy, or wavelength, respectively, is selected by a mechanical velocity selector with a resolution of typically 10% FWHM. Double pin-hole collimation tailors the beam for the necessary angular resolution, and a two-dimensional position sensitive detector registers the neutrons which are scattered to small angles around the incoming beam. The favored instrument is typically 40 m in length, 20 m for the collimation and 20 m for the secondary flight path with a flexible distance between sample position and detector. The detector sizes nowadays reach 96x96 cm^2 with about 16000 pixels of 7.5x7.5 mm^2 resolution. Electromagnets, cryomagnets, furnaces and cryostats, alone or in combination, belong generally to the standard equipment for sample environments.

At a pulsed source, like ISIS (UK) or IPNS (USA) [10], the concept of a SANS instrument is different, making use of a time-of-flight selection of the 'white' incoming beam. Besides that, the operational concept is very similar to instruments at continuous sources.

In the experiment the scattered intensity is registered as a function of the radial distance from the beam center, i.e. as a function of the scattering angle 2θ , or, more general, as function of the scattering vector **Q** or of its modulus Q. The latter is related to 2θ via $Q = (4\pi/\lambda) \sin \theta$, with λ, the neutron wavelength. By appropriate calibration one obtains the intensity in absolute units of the differential scattering cross section $(d\sigma/d\Omega)$ (Q). When the scattering is isotropic around the central beam, it may be averaged azimuthally for each value of Q (so-called "radial average"). If the scattering is non-isotropic, as often observed in the case of magnetic scattering, one has to consider the scattering in different azimuthal directions by sectional averaging.

For characterizing magnetic structures it is mostly necessary, or at least helpful, to analyze the response of the scattering to an externally applied magnetic field. In the examples treated in the present chapter such an external field, when applied, is assumed to be homogeneous, directing horizontally and perpendicular to the incident neutron beam. Other configurations are possible and can be adapted if appropriate, for instance, a beam-parallel field for investigating vortex lattices in superconductors. Such examples are not considered here, although the same theoretical principles as outlined in section 2 apply.

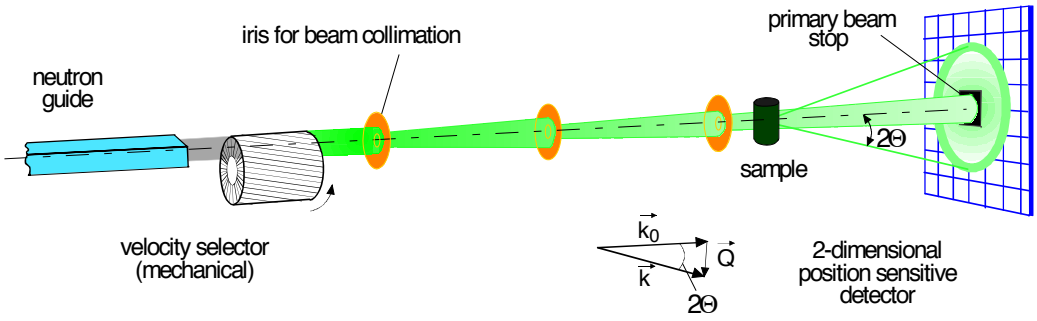

Figure 1: Schematic layout of a classical SANS facility at a continuous neutron source.

2. Neutron scattering

This section gives a general theoretical introduction to neutron scattering focusing to magnetic scattering and small angle scattering, with the objective to introduce the established notations and present and explain the most important basic formulae needed to evaluate a scattering experiment characterizing magnetic structures. For further reading and more details we refer to [11-20].

In a scattering experiment, the primary goal is a detailed analysis of the measured scattering pattern in relation to the properties of the incoming neutron beam. Monochromator and collimator define the energy (wavelength) and divergence of the incoming neutrons. Those interact with a sample and thereby undergo a momentum transfer $\hbar\mathbf{Q}$, with the scattering vector $\mathbf{Q}=\mathbf{k}_0-\mathbf{k}$, and $\mathbf{k}_0$, $\mathbf{k}$ being the wave vectors of the incoming and scattered neutrons, respectively. This process in principle can be elastic or inelastic. For small angle scattering inelastic scattering events are of minor importance and will be neglected in the present treatise.

2.1 Scattering potential

The scattering of a neutron, interacting through a scalar potential $V(\mathbf{r})$ with material, can be described by the asymptotic solution of the Schrödinger equation, see e.g. [11,12], which results in the wave function

$$\varphi_{\mathbf{k}_0}(\mathbf{r}) \xrightarrow[\mathbf{r}\to\infty]{} \frac{1}{(2\pi)^{3/2}}\left[e^{\imath\mathbf{k}_0\mathbf{r}} + f(\theta,\varphi)\frac{e^{\imath k_0 r}}{r}\right] \tag{1}$$

where $f(\theta,\varphi)$ in first Born approximation is given by

$$f(\theta,\varphi) = -\frac{m_N}{2\pi\hbar^2}\int d^3r\, e^{\imath\mathbf{Q}\mathbf{r}} V(\mathbf{r}) \tag{2}$$

For low-energy and short-ranging (i.e. nuclear) interactions the potential $V(\mathbf{r})$ can well be approximated by the Fermi pseudo-potential [13]

$$V(\mathbf{r}) = \frac{2\pi\hbar^2}{m_N} b_j \delta^3(\mathbf{r}-\mathbf{r}_j) \tag{3}$$

thus that $f(\theta,\varphi)$ reduces to

$$f(\theta,\varphi) = -b_j \tag{4}$$

b_j being the so-called atomic scattering length of atom j.

In this approximation, the differential scattering cross section per atom can be written as [14]

$$\frac{d\sigma}{d\Omega}(\mathbf{Q}) = \frac{1}{N}|f(\theta,\varphi)|^2 = \frac{1}{N}\left|\sum_{j=1}^{N} b_j \exp\left(i\mathbf{Q}\mathbf{r}_j\right)\right|^2 \tag{5}$$

where N is the number of atoms exposed to the beam.

2.2 Magnetic scattering

In the case of magnetic moments in the sample, the neutron undergoes a magnetic interaction in addition to the nuclear interaction. The corresponding interaction potential is given by [15]

$$V(\mathbf{r}) = -\boldsymbol{\mu}_N \cdot \mathbf{B}(\mathbf{r}) \text{ with } \boldsymbol{\mu}_N = \gamma \frac{e\hbar}{2m_N}\boldsymbol{\sigma} \tag{6}$$

where $\boldsymbol{\mu}_N$ is the magnetic dipole moment of the neutron, $\boldsymbol{\sigma}$ the Pauli spin operator, γ = -1.913 the gyromagnetic ratio and $\mathbf{B}(\mathbf{r})$ the magnetic field induced by an atom at the position of the neutron. The latter has two components, one induced by the magnetic dipole moment $\boldsymbol{\mu}_S$ of the electrons, denoted $\mathbf{B}_S(\mathbf{r})$, and one by their orbital moment $\boldsymbol{\mu}_L$, denoted $\mathbf{B}_L(\mathbf{r})$. The (weak) magnetic interaction $V(\mathbf{r}) = \boldsymbol{\mu}_N (\mathbf{B}_S(\mathbf{r}) + \mathbf{B}_L(\mathbf{r}))$ can as well be treated in first Born approximation, resulting in the magnetic scattering amplitude, in analogy to the nuclear scattering amplitude, given by the Fourier transform of the magnetic interaction potential

$$b_M = -\frac{m_N}{2\pi\hbar^2}\int d^3r\, e^{i\mathbf{Q}\mathbf{r}}\, \boldsymbol{\mu}_N \cdot \left(\mathbf{B}_S(\mathbf{r}) + \mathbf{B}_L(\mathbf{r})\right). \tag{7}$$

An additional static magnetic field $\mathbf{H}(\mathbf{r})$ at the point of local magnetization $\mathbf{M}(\mathbf{r})$ (originating from $\mathbf{B}_S(\mathbf{r}) + \mathbf{B}_L(\mathbf{r})$) induces a total local magnetic induction of

$$\mathbf{B}(\mathbf{r}) = \mu_0\left(\mathbf{H}(\mathbf{r}) + \mathbf{M}(\mathbf{r})\right) \tag{8}$$

and the Fourier transform of $\mathbf{B}(\mathbf{r})$ yields [cf. 16-18]

$$\mathbf{B}(\mathbf{Q}) = \mu_0 \frac{\mathbf{Q}\times\left[\mathbf{M}(\mathbf{Q})\times\mathbf{Q}\right]}{Q^2} = \mu_0\mathbf{M}_\perp(\mathbf{Q}) = \mu_0\mathbf{M}(\mathbf{Q})\sin\left(\angle(\mathbf{Q},\mathbf{M})\right) \tag{9}$$

where $\mathbf{M}(\mathbf{Q}) = \int d^3r \exp(i\mathbf{Q}\cdot\mathbf{r})\mathbf{M}(\mathbf{r})$, with $\mathbf{M}(\mathbf{r})$ given in units of Am.

$\mathbf{M}_\perp(\mathbf{Q}) = \mathbf{Q}\times\left[\mathbf{M}(\mathbf{Q})\times\mathbf{Q}\right]/Q^2 = \left|\mathbf{M}(\mathbf{Q})\right|\sin\left(\angle(\mathbf{Q},\mathbf{M})\right)$ is the magnetization component perpendicular to the scattering vector $\mathbf{Q}$. The magnetic scattering length then is [16]

$$b_M = \frac{\gamma e\mu_0}{2\pi\hbar}\boldsymbol{\sigma}\cdot\mathbf{M}_\perp(\mathbf{Q}) = D_M\mu_0\boldsymbol{\sigma}\cdot\mathbf{M}_\perp(\mathbf{Q}). \tag{10}$$

For the differential scattering cross section one finally obtains

$$\frac{d\sigma_M}{d\Omega}(\mathbf{Q}) = \frac{D_M^2}{N}\left|\mu_0 \mathbf{M}_\perp(\mathbf{Q})\right|^2 \tag{11}$$

2.3 Polarized neutron scattering

In the presence of a preferred direction, for example induced by an external magnetic field, the magnetic scattering depends on the spin state $\boldsymbol{\sigma}$ of the neutrons. Let the z-axis be the preferred direction, and let (+) and (–) denote the neutron spin polarizations parallel and antiparallel to the z-axis, then the scattering is described by four scattering processes: two processes where the incident states (+) and (–) remain unchanged (++ and – –), the so-called 'non-spin-flip' processes, and two processes where the spin is flipped (+– and –+), the 'spin-flip' processes. Keeping in mind that the nuclear scattering does not flip the neutron spin, the four related scattering lengths are [19]

$$b_{\pm\pm} = b_N \mp D_M \mu_0 M_{\perp z} \tag{12a}$$

$$b_{\pm\mp} = -D_M \mu_0 \left(M_{\perp y} \pm i M_{\perp x}\right) \tag{12b}$$

It is evident that non-spin-flip scattering only contains magnetic contributions from effective magnetization components along the z-axis. If the scattering vector $\mathbf{Q}$ is parallel to the z-axis, $M_{\perp z}$ is zero. On the other hand, if spin-flip scattering is present, it is exclusively due to effective magnetic components deviating from the z-axis, the axis of magnetic polarization.

For an unpolarized neutron beam (which may be taken composed of 50% (+) and 50% (–) polarization) the square of the modulus of the scattering length is

$$\left|b\right|^2 = \frac{1}{2}\left(b_{++}^2 + b_{--}^2 + \left|b_{+-}\right|^2 + \left|b_{-+}\right|^2\right) = b_N^2 + D_M^2\left|\mu_0 \mathbf{M}_\perp\right|^2 \tag{13}$$

The differential cross section of the unpolarized neutron beam can therefore be described by the sum of the nuclear and the magnetic cross section, without any cross terms.

2.4 Small angle neutron scattering

2.4.1 Scattering by individual magnetic particles

Small angle scattering does not resolve individual atoms, but structures of sizes in the nanometer range. Therefore the discrete atomic scattering lengths b_j can be replaced by a scattering length density $\rho(\mathbf{r})$ of the sample. The differential scattering cross-section (c.f. Eq. (5)) is than given by the Fourier transform of $\rho(\mathbf{r})$:

$$\frac{d\sigma}{d\Omega}(\mathbf{Q}) = \frac{1}{V}\left|\int_V d^3r\,\rho(\mathbf{r})e^{i\mathbf{Q}\cdot\mathbf{r}}\right|^2 \tag{14}$$

with V being the sample volume. Assuming that this volume contains N particles embedded in a surrounding matrix of constant scattering cross section ρ_{matrix} , we define the scattering length distribution inside each particle by $\rho_{P,j}(\mathbf{r})=\Delta\eta_j(\mathbf{r})+\rho_{\text{matrix}}$. Than, with $\mathbf{R}_j$ being the vector pointing to the centre of the particle j, the related scattering cross section can be written as

$$\frac{d\sigma}{d\Omega}(\mathbf{Q}) = \frac{1}{V}\left|\sum_{j=1}^{N} F_j(\mathbf{Q})\,e^{i\mathbf{Q}\mathbf{R}_j}\right|^2 \quad \text{with} \quad F_j(\mathbf{Q}) = \int_{V_j(\mathbf{R}_j)} d^3r\,\Delta\eta_j(\mathbf{r})\; e^{i\mathbf{Q}(\mathbf{r}-\mathbf{R}_j)} \tag{15}$$

For particles of constant scattering length density, the scattering amplitude for nuclear scattering can be expressed as

$$F_N(\mathbf{Q}) = \Delta b_N V_P f(\mathbf{Q}). \tag{16}$$

where the constant $\Delta\eta_j$ was replaced by Δb_N , the contrast for nuclear scattering between the particles and the surrounding matrix. V_P is the particle volume. $f(\mathbf{Q})$ denotes the so-called particle formfactor and can be calculated analytically for many simple particle shapes, as tabulated in [20]. For spherical particles of radius R, it is the well-known expression, dating back to Lord Rayleigh [21]

$$f(QR) = 3\frac{\sin(QR) - QR\cos(QR)}{(QR)^3}. \tag{17}$$

We now assume the same particles being of homogenous magnetisation $\mathbf{M}_P$, embedded in a homogenously magnetized surrounding $\mathbf{M}_M$. The magnetic scattering of these particles then depends on the magnetic contrast vector $\Delta\mathbf{M}= \mathbf{M}_P-\mathbf{M}_M$ relative to the scattering vector $\mathbf{Q}$:

$$\mathbf{M}_\perp = \frac{\mathbf{Q}\times(\Delta\mathbf{M}\times\mathbf{Q})}{Q^2} \tag{18}$$

To calculate the magnetic scattering amplitude one has to consider the spin state before and after the scattering process according to Eqs. (12a,b)

$$F_{\pm\pm}(\mathbf{Q}) = \Delta b_{\pm\pm} V_P f(\mathbf{Q}) \;, \qquad F_{\pm\mp}(\mathbf{Q}) = \Delta b_{\pm\mp} V_P f(\mathbf{Q}) \tag{19}$$

2.4.2 Scattering by groups of particles

The scattering from an accumulation of many particles is obtained by summing up the scattering amplitudes of all particles weighted by a phase shift at each particle position. The general expression for the scattering cross section then is given by

$$\frac{d\sigma_j}{d\Omega}(Q) = \left\langle F_j^2(Q)\right\rangle + \left\langle F_j(Q)\right\rangle^2 (S(Q)-1) \tag{20}$$

(j standing for $\pm\pm$, $\pm\mp$, or N and M in the case of unpolarized neutrons, respectively). The right-hand-side of Eq. (20) consist of two terms: The first one depends only on the particle structure and corresponds to the independent scattering of N particles, while the second one considers their spatial distribution and reflects the interparticle interference described by $S(\mathbf{Q})$. The $\langle\ \rangle$ indicates an average over all possible configurations and sizes of the particles.

As postulated by Eq. (13), in the case of an unpolarized incident neutron beam the scattering of both contributions, nuclear and magnetic, is linearly superposed

$$\frac{d\sigma_{unp}}{d\Omega}(\mathbf{Q}) = \frac{d\sigma_N}{d\Omega}(\mathbf{Q}) + \frac{d\sigma_M}{d\Omega}(\mathbf{Q}) \tag{21}$$

In both contributions two averages are involved: the average of the squared scattering function and the square of the average scattering function. For monodisperse, radially symmetric particles, for nuclear scattering the averages $\left\langle F_N^2(Q)\right\rangle \equiv \left\langle F_N(Q)\right\rangle^2$ are identical, so that

$$\frac{d\sigma_N}{d\Omega}(Q) = F_N^2(Q)S(Q) \tag{22}$$

To evaluate the averages for the magnetic scattering cross-section we have to consider the angular orientations of $\Delta\mathbf{M}$, parameterized by the angular alignment probability $p(\varphi_M, \Theta_M)$ of $\Delta\mathbf{M}$. Following up Eq. (11), the averages over all $p(\varphi_M, \Theta_M)$ are than given by the general expressions

$$\left\langle F_M^2(Q)\right\rangle = V_P^2 f^2(Q,R)\int p(\varphi_M,\Theta_M)\left[D_M \mu_0 \mathbf{M}_\perp(\mathbf{Q})\right]^2 d\varphi_M d\Theta_M \tag{23a}$$

$$\left\langle F_M(Q)\right\rangle^2 = \left[\int p(\varphi_M,\Theta_M) V_P f(Q,R) D_M \mu_0 \mathbf{M}_\perp(\mathbf{Q}) d\varphi_M d\Theta_M\right]^2 \tag{23b}$$

For two extremes, i.e. a demagnetised sample ($\Delta\mathbf{M}$ at random orientation) and a sample in magnetic saturation ($\Delta\mathbf{M}$ all parallel), the averages can readily be performed:

In the case of random orientation of $\Delta\mathbf{M}$ the square of the average formfactor $\left\langle F_M(\mathbf{Q})\right\rangle^2$ is zero and

$$\frac{d\sigma_M}{d\Omega}(\mathbf{Q}) = \left\langle F_M^2(\mathbf{Q})\right\rangle = \frac{2}{3}(D_M \mu_0 \Delta M)^2 V_P^2 f^2(\mathbf{Q}) \tag{24}$$

which is independent of interparticle interference effects.

In the case of magnetic saturation, the averages $\left\langle F_M^2(\mathbf{Q})\right\rangle \equiv \left\langle F_M(\mathbf{Q})\right\rangle^2$ are identical, as for nuclear scattering, and we obtain

$$\frac{d\sigma_M}{d\Omega}(\mathbf{Q}) = (D_M \mu_0 \Delta M)^2 V_P^2 f^2(\mathbf{Q}) \sin^2(\Psi) \tag{25}$$

where $\Psi = \angle(\mathbf{Q}, \Delta\mathbf{M})$, the angle between the direction of the magnetic contrast $\Delta\mathbf{M}$, and the scattering vector $\boldsymbol{Q}$, in practice the azimuthal angle on the two-dimensional SANS detector.

Averaging with regard to the azimuthal angle results in

$$\frac{d\sigma_M}{d\Omega}(\mathbf{Q}) = \frac{1}{2}(D_M \mu_0 \Delta M)^2 V_P^2 f^2(\mathbf{Q}) \tag{26}$$

which differs from Eq (24) only by the prefactor 1/2 instead of 2/3.

If the particles are not monodisperse in size, and/or not equal in shape, each size/shape class has to be considered individually. When interparticle interference can be neglected, the scattering contributions of the different classes are incoherently superposed. In the particular case of a finite size distribution of equally shaped particles, neglecting interparticle interference, the scattering cross section can be calculated as the integral over all individual contributions from the size interval between R and $R + dR$. For the nuclear scattering, this results in

$$\frac{d\sigma_N}{d\Omega}(\mathbf{Q}) = \Delta b_N^2 \int_R f^2(\mathbf{Q}) V_P^2(R) N(R) dR \tag{27}$$

with $N(R)\ V_P(R)\ dR$ being the incremental volume fraction with $V_P(R)$, the particle volume in the related size interval.

For the magnetic scattering of particles of finite size distribution and in magnetic saturation, the scattering cross section is given in analogy to Eq. (27) by

$$\frac{d\sigma_M}{d\Omega}(\mathbf{Q}) = (D_M \mu_0 \Delta M)^2 \sin^2\Psi \int_R f^2(\mathbf{Q}) V_P^2(R) N(R) dR \tag{28}$$

2.4.3 SANS from superparamagnetic particles

A further example where the average over all orientations of the magnetic contrast can be treated analytically is the case of superparamagnetic particles. Since the same model, in adapted versions, holds to explain many of the scattering patterns in the successional examples we will discuss this case here in some more detail.

The superparamagnetic state is characterized as an ensemble of non-interacting magnetic particles, the magnetic orientation of each particle being governed by the balance between the thermal energy $E_{th} = kT$ and the potential energy of a magnetic particle imposed by an external magnetic field. The potential energy of a homogenously magnetized, single domain particle of magnetic moment $\boldsymbol{\mu}_P = \mathbf{M}_P V_P$ in a magnetic field $\mathbf{H}$ is $E_{\text{pot}} = -\mu_0 \mathbf{H} \cdot \mathbf{M}_P V_P$. Since the relaxation time for reaching the thermodynamic equilibrium is short compared to the SANS measuring time, the scattering cross-section of an ensemble of superparamagnetic particles can be calculated as thermodynamic equilibrium state following the Langevin statistics, as outlined in the following.

To calculate the averages according to Eqs. (23a,b), the orientation probability of the magnetic contrast $\Delta\mathbf{M}$ and its magnitude needs to be known. In the case of a classical superparamagnet, where magnetic single domain particles are embedded in a non-magnetic matrix, the magnetic contrast is identical to the magnetisation of the particle $\Delta\mathbf{M} = \mathbf{M}_P$, and the orientation distribution of the magnetic moments are following the Boltzmann statistics. When a magnetic field $\mathbf{H}$ is applied, it forces the magnetic moments $\boldsymbol{\mu}_P = \mathbf{M}_P V_P$ of the particle (see Figure 2a) to rotate towards the direction of $\mathbf{H}$. This tendency is opposed to disturbances by the thermal excitation. The probability p for a given orientation is then given by the Boltzmann factor

$$p = p_0 \exp\left(\mu_0 \mathbf{H} \cdot \mathbf{M}_P V_P / kT\right). \tag{29}$$

This model of a classical superparamagnet can be extended by allowing for a magnetic matrix surrounding the magnetic particle. For our treatment we assume a homogeneously magnetized matrix, i.e. a matrix in which the magnetisation is constant in magnitude and always parallel to the applied magnetic field $\mathbf{H}$, as illustrated in Figure 2b. The magnetic property of the matrix enters the scattering problem at two points. Firstly, the scattering contrast is now defined as the vector difference between the particle and the matrix $\Delta\mathbf{M} = \mathbf{M}_P - \mathbf{M}_M$, and secondly, the magnetic matrix influences the potential energy of the particle and therefore the magnetic orientation distribution. The influence on the orientation distribution depends strongly on the magnetic coupling between matrix and particle. If we assume that there is only magneto-static coupling, and no exchange coupling between particle and matrix, the magnetization of the matrix simply amplifies the external magnetic field such that the Boltzmann factor has to be modified accordingly, and the orientation probability is given as

$$p = p_0 \exp\left(\mu_0 \left(\mathbf{H} + \mathbf{M}_M\right) \cdot \mathbf{M}_P V_P / kT\right). \tag{30}$$

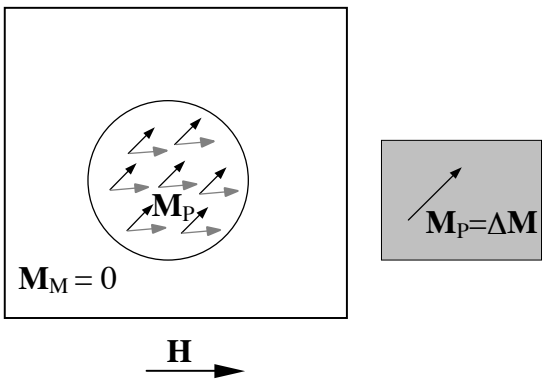

(a)

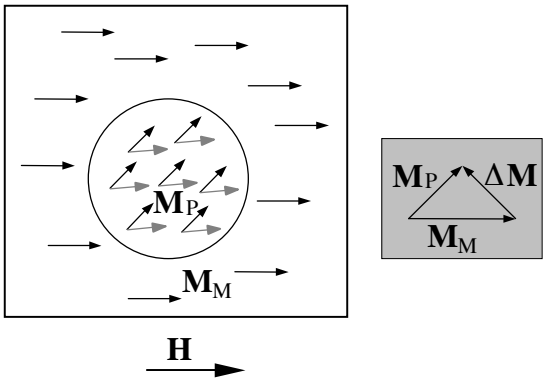

(b)

Figure 2: Schematic illustration of a superparamagnetic particle in an external external field **H**, embedded in a nonmagnetic matrix (a) or in a homogeneous magnetic matrix with the magnetization direction aligned parallel to **H** (b). The corresponding magnetic scattering contrast vectors $\Delta\mathbf{M} = \mathbf{M}_P - \mathbf{M}_M$ are illustrated in the shaded boxes.

Describing the orientation distribution of the magnetization of the particle $\mathbf{M}_P$ by the Boltzmann factor as in Eq. (30), the averages of the formfactors $\left\langle F_j^2(Q)\right\rangle$ and $\left\langle F_j(Q)\right\rangle^2$ can be calculated. For this purpose it is convenient to define the scattering vector **Q** and the magnetization of the particle $\mathbf{M}_P$ in polar coordinates as illustrated in Figure 3. Here, the $\mathbf{e}_x$-direction is assumed to be the direction of the incident neutron beam. The applied magnetic field **H** (and hence the magnetization of the matrix $\mathbf{M}_M$) are assumed to be parallel to $\mathbf{e}_z$. The 2-dimensional neutron detector is placed in the $\mathbf{e}_y\mathbf{e}_z$-plane. Then the relevant vectors are defined as

$$\mathbf{Q} = Q\begin{pmatrix}\cos\delta\\ \sin\delta\sin\Psi\\ \sin\delta\cos\Psi\end{pmatrix} \qquad \mathbf{M}_P = M_P\begin{pmatrix}\sin\Theta\cos\Phi\\ \cos\Theta\cos\Phi\\ \cos\Theta\end{pmatrix} \quad \mathbf{M}_M = \begin{pmatrix}0\\0\\M_M\end{pmatrix} \quad \mathbf{H} = \begin{pmatrix}0\\0\\H\end{pmatrix}$$

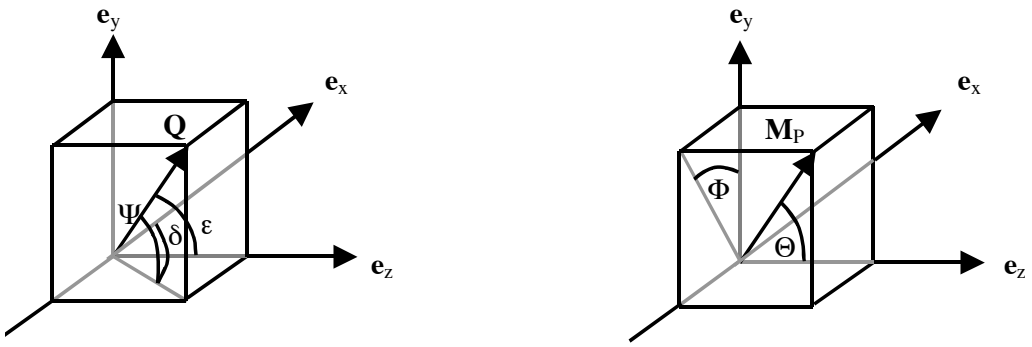

Figure 3: Definition of the scattering vector **Q** and the particle magnetization $\mathbf{M}_P$ in polar coordinates.

The averages of the formfactors for the different spin states (cf. Eq. (19)) can be written as

$$\left\langle F^2_{\substack{\pm\pm \\ \pm\mp}}(\mathbf{Q})\right\rangle = \int_0^{2\pi}\int_0^{\pi} 4\pi \sin\Theta\, p_0 e^{\mu_0 (H+M_M) M_P V_P \cos\Theta / kT} \left(\Delta b_{\substack{\pm\pm \\ \pm\mp}} V_P f(\mathbf{Q}) \right)^2 d\Theta\, d\Phi \qquad (31a)$$

$$\left\langle F_{\substack{\pm\pm \\ \pm\mp}}(\mathbf{Q})\right\rangle^2 = \left(\int_0^{2\pi}\int_0^{\pi} 4\pi \sin\Theta\, p_0 e^{\mu_0 (H+M_M) M_P V_P \cos\Theta / kT} \Delta b_{\substack{\pm\pm \\ \pm\mp}} V_P f(\mathbf{Q}) d\Theta\, d\Phi \right)^2 \qquad (31b)$$

The Boltzmann factor p is normalized to unity by choosing the normalization factor $p_0 = \left[(4\pi)^2 \sinh(\alpha)/\alpha\right]^{-1}$ with the α–parameter representing the ratio between magnetic (potential) and thermal energy:

$$\alpha = \mu_0 (H + M_M) M_P V_P / kT \qquad (32)$$

The averages can be calculated analytically: Combining Eqs. 12, 18, 19, 20 and 31 and introducing the classical Langevin-function $L(\alpha) = \coth\alpha - 1/\alpha$, after some calculations one obtains the scattering cross-section of a superparamagnetic particle system in a homogeneous magnetic matrix described by the expressions

$$\begin{aligned} \frac{d\sigma_{\pm\pm}}{d\Omega}(\mathbf{Q}) = & \left(F_N(\mathbf{Q}) \mp \tilde{F}_M(\mathbf{Q}) \left[L(\alpha) - \gamma \right] \sin^2\varepsilon \right)^2 S(\mathbf{Q}) \\ & + \tilde{F}_M^2(\mathbf{Q}) \left(\frac{L(\alpha)}{\alpha} \sin^2\varepsilon - \left(L^2(\alpha) - 1 + 3\frac{L(\alpha)}{\alpha} \right) \sin^4\varepsilon \right) \end{aligned} \qquad (33a)$$

$$\begin{aligned} \frac{d\sigma_{\pm\mp}}{d\Omega}(\mathbf{Q}) = & \left(\sin^2\varepsilon - \sin^4\varepsilon \right) \left[L(\alpha) - \gamma \right]^2 \tilde{F}_M^2(\mathbf{Q})\, S(\mathbf{Q}) \\ & + \tilde{F}_M^2(\mathbf{Q}) \left(\left(\sin^2\varepsilon - \sin^4\varepsilon \right) \left(L^2(\alpha) - 1 + 3\frac{L(\alpha)}{\alpha} \right) + \left(2 - \sin^2\varepsilon \right) \frac{L(\alpha)}{\alpha} \right) \end{aligned} \qquad (33b)$$

$$\begin{aligned} \frac{d\sigma_{unp}}{d\Omega}(\mathbf{Q}) &= \frac{1}{2} \left(\frac{d\sigma_{++}}{d\Omega}(\mathbf{Q}) + \frac{d\sigma_{--}}{d\Omega}(\mathbf{Q}) + \frac{d\sigma_{+-}}{d\Omega}(\mathbf{Q}) + \frac{d\sigma_{-+}}{d\Omega}(\mathbf{Q}) \right) \\ &= \left(\tilde{F}_M^2(\mathbf{Q}) \left[L(\alpha) - \gamma \right]^2 \sin^2\varepsilon + F_N^2(\mathbf{Q}) \right) S(\mathbf{Q}) \\ &+ \tilde{F}_M^2(\mathbf{Q}) \left(2\frac{L(\alpha)}{\alpha} - \left(L^2(\alpha) - 1 + 3\frac{L(\alpha)}{\alpha} \right) \sin^2\varepsilon \right) \end{aligned} \qquad (33c)$$

$\tilde{F}_M(\mathbf{Q}) = \mu_0 D_M M_P V_P f(\mathbf{Q})$ and $F_N(\mathbf{Q}) = \Delta b_N V_P f(\mathbf{Q})$ are the magnetic and nuclear scattering amplitudes, respectively. γ is defined as $\gamma = M_M / M_P$, and ε is the angle between $\mathbf{Q}$ and $\mathbf{e}_z$, which in practice is the same as Ψ ($\cos\varepsilon = \sin\delta\cos\Psi \approx \cos\Psi$ for $\delta \approx \pi/2$).

If all formfactors $f(\mathbf{Q})$ only depend on the modulus of the scattering vector, Q, the scattering cross-sections can be written in the form

$$\frac{d\sigma}{d\Omega}(Q) = A(Q) + B(Q)\sin^2\Psi + C(Q)\sin^4\Psi \tag{34}$$

whereby for unpolarized neutrons the last term vanishes, i.e. $C(Q) \equiv 0$. Eqs. (33) describe the transition of the magnetic scattering contribution from an anisotropic (ψ-dependent) to an istotropic (ψ-independent) scattering behavior when increasing the disorder of the magnetic moments. From Eqs. (33) one obtains immediately the limiting cases of saturation and complete disorder:

For large values of α, i.e. high magnetic fields and/or low temperatures such that all magnetic moments are uniformly aligned, we obtain $\lim_{\alpha\to\infty} {}^{L(\alpha)}/_{\alpha} = 0$ and $\lim_{\alpha\to\infty} L(\alpha) = 1$, and the isotropic magnetic scattering term $\tilde{F}_M^2(Q)2L(\alpha)/\alpha$ vanishes. Hence, the magnetic scattering gets fully anisotropic, only the nuclear scattering remains isotropic. For unpolarized neutrons the two remaining terms in Eq. (34), *A(Q)* and *B(Q)*, then are given by the expressions

$$\begin{aligned} \lim_{\alpha\to\infty} A_{unp}(Q) &= \left|F_N(Q)\right|^2 S(Q) \\ \lim_{\alpha\to\infty} B_{unp}(Q) &= D_M^2 \mu_0^2 \Delta M^2 V_P^2 f^2(Q) S(Q) \end{aligned} \tag{35}$$

For small values of α, i.e. high temperatures and/or low magnetic fields, we get the other limiting case where $\lim_{\alpha\to 0} {}^{L(\alpha)}/_{\alpha} = 1/3$ and $\lim_{\alpha\to 0} L(\alpha) = 0$ and hence, the magnetic scattering contributes by 2/3 of its magnitude to the isotropic scattering:

$$\lim_{\alpha\to 0} A_{unp}(Q) = \left|F_N(Q)\right|^2 S(Q) + \frac{2}{3}\tilde{F}_M^2(Q)\,. \tag{36}$$

For unpolarized neutrons and for random orientation of the magnetic moments of the particles the unisotropic term converges towards

$$\lim_{\alpha\to 0} B_{unp}(Q) = \gamma^2 \tilde{F}_M^2(Q) S(Q) = D_M^2 \mu_0^2 M_M^2 V_P^2 f^2(Q) S(Q) \tag{37}$$

This contribution only vanishes for random magnetic orientation of particles in a nonmagnetic (or paramagnetic) matrix ($M_M = 0 \Rightarrow \gamma = 0$), because only in that case the average magnetic contrast is zero, i.e. $\langle \Delta \mathbf{M} \rangle = 0$.

The scattering behavior of a system of superparamagnetic particles in many aspects is very typical for other systems of micromagnetism, as treated by the examples in Section 3, and can be a valuable basis for the interpretation of the observed scattering. Therefore, in preparation of Section 3 Figure 4 shows simulated examples of magnetic scattering patterns from superparamagnetic particles on a two-dimensional SANS detector. The simulations were made on the basis of Eq. (33c), i.e. for the case of an unpolarized neutron beam. For the simulations nuclear scattering has been neglected. The latter, if present, would be isotropic and linearly superposed. Figure 4 distinguishes examples for magnetic particles in a nonmagnetic matrix, cf. Figure 2a (γ=0), and in a magnetic matrix, cf. Figure 2b, for the latter assuming in magnitude the same magnetization as for the particles (γ=1). Varying the Langevin parameter α from 0 to ∞ simulates the transition from fully random magnetic orientation of the particles to a strong field-parallel alignment.

For γ=0 (nonmagnetic matrix) the scattering patterns show the classical transition from being isotropic for α=0 to passing a vertical (field-perpendicular) elliptical distortion for intermediate α (note that the hypothetical magnetic field is directing horizontally) and finally, for large α, showing the $\sin^2\psi$ behavior expected from Eq. (25). On the other hand, in a magnetic matrix (γ=1) the patterns are quite different: Here, the resulting net magnetic contrast $\Delta\mathbf{M} = \mathbf{M}_P - \mathbf{M}_M$, initially governed by the field-parallel matrix, develops a residual field-perpendicular component (cf. shaded inset in Figure 2b). Consequently, the scattering patterns show a vertical $\sin^2\psi$ behavior for small α, passing nearly isotropic patterns for intermediate α, and finally converting into a horizontal (field-parallel) elliptical elongation. When approaching saturation ($\alpha \rightarrow \infty$) the magnetic contrast reduces to zero in this case and the magnetic scattering vanishes.

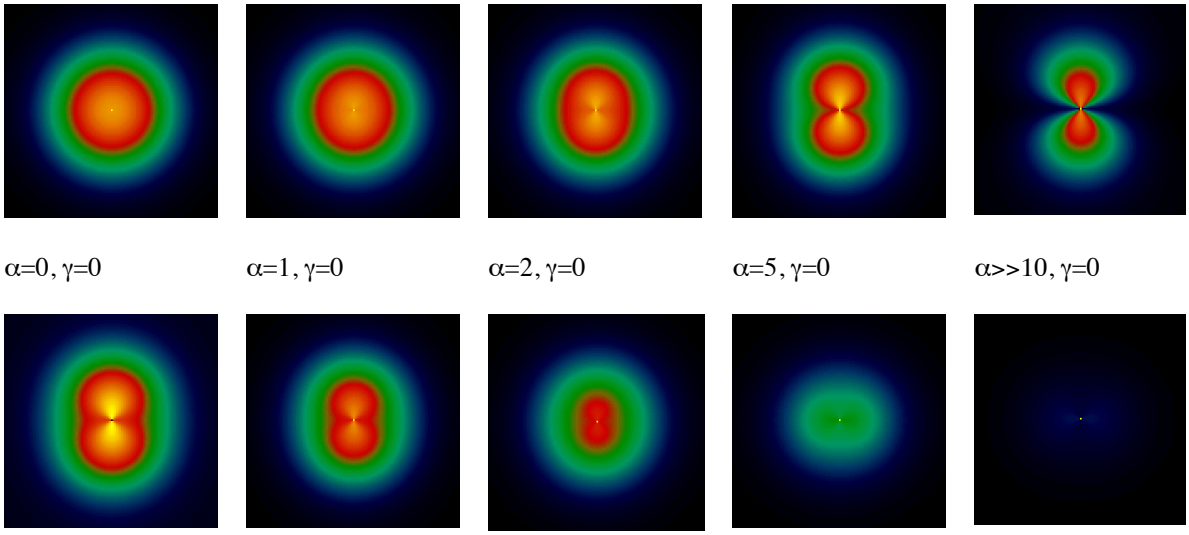

Figure 4: Simulated 2-dimensional magnetic SANS patterns of superparamagnetic particles in a nonmagnetic matrix (γ=0) and in a magnetic matrix of the same magnetic moment in magnitude as that of the particles (γ=1), in both cases for an unpolarized incident neutron beam. Varying the Langevin parameter α from 0 to ∞ simulates the transition from fully random magnetic orientation of the particles to a strong field-parallel alignment (the hypothetic field is directing horizontally).

3. References

[1] V. F. Sears, Neutron News **3** (1992) 26, L. Koester, H. Rauch, M. Herkens, K. Schröder, Report of the Research Centre Jülich (FZJ), Germany, ISSN 0366-0885, IAEA-Contract 2517/RB (1981), G.E.Bacon, 'Neutron Diffraction', Clarendon Press, Oxford (1975)

[2] CRC Handbook of Chemistry and Physics, ed. R. C. Weast, CRC Press, Florida, E-107

[3] C.G. Shull and M.K. Wilkinson, Phys. Rev. **97** (1955) 304

[4] K. Ibel, J. Appl. Cryst. **9** (1976) 296

[5] H. R. Child, S. Spooner, J. Appl. Cryst. **13** (1980) 259

[6] J. Kohlbrecher and W. Wagner, J. Appl. Cryst **33** (2000) 804

[7] T. Keller, T. Krist, A. Danzig, U. Keiderling, F. Mezei, A. Wiedenmann, Nuclear Instruments and Methods in Physics Research A 451 (2000) 474-479

[8] J. Zhao, W. Meerwinck, T. Niinikoski, A. Rijllart, M. Schmitt, R. Willumeit and H. Stuhrmann, Nuclear Instruments and Methods in Physics Research A 356 (1995) 133-137

[9] H. Glättli, M. Eisenkrämer, M. Pinot and C. Fermon, Physica B 213&214 (1995) 887-888

[10] P. Thiyagarajan, J. E. Epperson, R. K. Crawford, J. M. Carpenter, T. E. Klippert and D. G. Wozniak, J. Appl. Cryst. **30** (1997) 280

[11] O. Hittmair, "Lehrbuch der Quantentheorie", Karl Thiemig publishing (1972)

[12] J. Byrne, Neutrons, Institute of Physics Publishing, Bristol (1994), Chap. 2

[13] E. Fermi, Ric. Sci **7** (1936) 13

[14] G. Kostorz and S.W. Lovesey, in Treatise on Materials Science and Technology (Vol. **15**: Neutron Scattering), edited by G. Kostorz, Academic Press, New York, 1979, 22

[15] J. Rossat-Mignot, Neutron Scattering, Vol **23**, Part C (1997) Academic Press

[16] G.L. Squires, Cambridge University Press (1978)

[17] I.I. Gurevich and L.V. Tarasov, North Holland Publishing Company, Amsterdam (1968)

[18] W. Schmatz, in Treatise on Materials Science and Technology (Vol. 2), edited by H. Herman Academic Press, New York (1973), 128

[19] R.M. Moon, T. Riste, W.C. Koehler, Phys. Rev. **181** (1969) 920

[20] J.S. Pedersen, Advances in Colloid and Interface Science **70** (1997) 171

[21] O. M. Lord Rayleigh, Proc. R. Soc. London, A **84** (1911) 25

[22] A. Wiedenmann, J. Appl. Cryst. **33** (2000) 428

[23] A. Wiedenmann, Physica B **297** (2001) 226

[24] A. Wiedenmann, A. Hoell, M. Kammel, Journal of Magnetism and Magnetic Materials **252** (2002) 83

[25] A. Heinemann, A. Wiedenmann, J. Appl. Cryst. **36** (2003) 845

[26] A. Hoell, M. Kammel, A. Heinemann, A. Wiedemann J. Appl. Cryst. **36** (2003) 558

[27] J. R. Weertman, *Mechanical Behaviour of Nanocrystalline Metals in Nanostructured Materials: Processing, Properties, and Potential Applications*. (William Andrew Publishing, Norwich, 2002)

[28] Papers in special issue dedicated to Prof. H. Gleiter of Zeitschrift für Metallkunde, 10 (2003)

[29] H. Van Swygenhoven, *Science* **296,** 66 (2002

[30] W. Wernsdorfer, E.B. Orozco, K. Hasselbach, A. Benoit, B. Barbara, N. Demoncy, A. Loiseau, H. Pascard and D. Mailly, *Phys. Rev. Lett.* **78** (1997) 1791-1794

[31] Y. Yoshizava, S. Oguma and K. Yamauchi, *J. Appl. Phys.* **64** (1988) 6044-6064

[32] J.F. Löffler, J.P. Meier, B. Doudin, J.-P. Ansermet, W. Wagner, *Phys. Rev. B* **57** (1998) 2915

[33] J. F. Löffler, W. Wagner, H. van Swygenhoven, A. Wiedenmann, J. Nanostructured Materials **9** (1997) 331

[34] J.F. Löffler, H.B. Braun, and W. Wagner, *Phys. Rev. Lett.* **85** (2000) 1990

[35] J. F. Löffler, H. B. Braun, W. Wagner, G. Kostorz, A. Wiedenmann, Mater. Sci. Eng. A **14195**, (2000) 1

[36] W. Wagner, J. Kohlbrecher, J. F. Löffler, Materials Week, www.materialsweek.org/proceedings, mw2000_433.pdf (2001)

[37] H. Gleiter, *Progress in Material Science* **33**, 223, (1989)

[38] P. Fratzl, J. L. Lebowitz, J. Marro, and M. H. Kalos, Acta Metall **31** (1983) 1849

[39] B. Hofmann, T. Reininger, H. Kronmüller, *Phys. Stat. Sol.* (a) **134** (1992) 247

[40] A. Hernando, M. Vazquez, T. Kulik, C. Prados, *Phys. Rev. B* **51** (1995) 3581

[41] W. Wagner, A. Wiedenmann, W. Petry, A. Geibel and H. Gleiter, *J. Mater. Res.* **6** (1991) 2305

[42] J.A. Michels et al, *Phys. Status Solidi* A **189**, (2002) 509

[43] J. Weissmüller, D. Michels, A. Michels, A. Wiedenmann, C.E. Krill, H.M. Sauer and R. Birringer *Scripta Materialia* **44**, (2001) 2357-2361

[44] A. Michels et al., *Phys. Rev. Lett.* **91**, No 26 (2004)

[45] J. Degauque, B. Astié, J. L. Porteseil and R. Vergne, *J. Magn. Magn. Mater.* **26** (1982) 261

[46] F. Pfeifer and C. Radeloff, *J. Magn. Magn. Mater.* **19** (1980) 190

[47] A. Mager, Ann. Phys. (Leipzig) **11** (1952) 15

[48] R. Przenioslo, R. Winter, H. Natter, M. Schmelzer, R. Hempelmann, W. Wagner, Phys. Rev. B **63** (2001) 054408

[49] R. Przenioslo, J. Wagner, H. Natter, R. Hempelmann, W. Wagner, Journal of Alloys and Compounds **328** (2001) 259

[50] G. Herzer, *IEEE Trans. Mag.* **25** (1989) 3327

[51] J. Kohlbrecher, A. Wiedenmann, H. Wollenberger, *Z. Phys. B* **104** (1997) 1

[52] A. R. Yavari, G. Fish, S. K. Das, and L. A. Davis, Mat. Sci. Eng. **A182/A183**, 1415 (1994), A. R. Yavari and O. Drbohlav, *Mat. Trans. JIM* **36** (1995) 896

[53] A. Heinemann, H. Hermann, A. Wiedenmann, N. Mattern and K. Wetzig, J. Appl. Cryst. **33** (2000) 1386

[54] Y.-Y Chuang, R. Schmid, and Y. Austin-Chang, Acta metall. **33** (1985) 1369

[55] R. Wagner in 'Crystals', Vol. 6, Springer Verlag, Berlin (1982)

[56] W. Wagner, R. Lang, H. Wollenberger, and W. Petry, in "Phase Transformation '87", Ed. G.W.Lorimer, The Institute of Metals, 566 (1988); W. Wagner, Mat. Sci. Forum **27/28**, 413 (1988)

[57] R. P. Wahi and J. Stajer, in 'Decomposition of Alloys: the early stages', eds. P. Hasen et al., Pergamon Press (1984) 165

[58] O. Lyon and J. P. Simons, J. Phys.: Condens. Matter **4** (1992) 6073

[59] O. Lyon and J. P. Simons, J. Phys.: Condens. Matter **6** (1994) 1627

[60] L. Delannay, O. V. Mishin, D. Juul Jensen and P. van Houtte, Acta Mater. **49** (2001) 2441